Cent. Eur. J. Phys. • 6(3) • 2008 • 427-433
DOI: 10.2478/s11534-008-0068-3

VERSITA

Central European Journal of **Physics**

Motion of spiral waves induced by local pacing

Research Article

Jiang-Xing Chen[1]*, Gui-Na Wei[2], Bing-Wei Li[3]†, Jiang-Rong Xu[1]

1 *Department of physics, Hangzhou Dianzi University, Hangzhou 310018, China*

2 *The Second Affiliated Hospital, School of Medicine, Zhejiang University, Hangzhou 310009, China*

3 *Department of Physics, Zhejiang University, Hangzhou 310027, China*

Received 7 November 2007; accepted 25 February 2008

Abstract: The motion of spiral waves in excitable media driven by a weak pacing around the spiral tip is investigated numerically as well as theoretically. We presented a Bifurcations diagram containing four types of the spiral motion induced by different frequencies of pacing: rigidly rotating, inward-petal meandering, resonant drift, and outward-petal meandering spiral. Simulation shows that the spiral resonantly drifts when the frequency of pacing is close to that of the spiral rotation. We also find that the speed and direction of the drift can be efficiently controlled by means of the strength and phase of the local pacing, which is consistent with analytical results based on the framework of the weak deformation approximation.

PACS (2008): 47.54.Fj, 87.19.Hh, 82.40.Ck

Keywords: spiral wave • local pacing • resonant drift • weak deformation approximation

1. Introduction

Spiral wave is one of the most typical two-dimensional spatiotemporal patterns in excitable media which has been observed and studied in many different biological [1–4], physical [5, 6], chemical [7–10], and mathematical model systems [11, 12]. In particular, spiral waves of excitation in heart tissue underlie certain types of dangerous cardiac arrhythmias such as ventricular tachycardias and fibrillation [13, 14]. Thus, a crucial topic has been devoted to putting forward various methods to control spiral waves and spiral turbulence [15, 16].

The current clinical method of large amplitude shocks applied in performing cardiac defibrillation [17, 18], may damage the cardiac tissues and cause serious pains. There are growing experimental and theoretical efforts to develop low amplitude defibrillation methods in both fields of nonlinear science and cardiac physiology [18–21]. A so-called local and low-amplitude pacing control scheme has become a promising method for defibrillation in cardiac tissue [22, 23].

In addition to the attention given to the suppressing turbulence, manipulating the spiral drift is another efficient controlling strategy. It is based on the fact that once the rotating spiral center is driven to a boundary (e.g., heart's surface), spiral waves are no longer sustained and they will vanish eventually. Because of its fundamental and potential practical importance, many studies have been carried out to understand or manipulate the motion of the spiral tips under various situations such as external ex-

*E-mail: jxchen@zimp.zju.edu.cn
†E-mail: bwelllee@zju.edu.cn

citation waves [24], periodic illumination [25, 26], a parameter gradient [27] as well as dc and ac electric fields [28, 29]. It is [30] pointed out that when forced frequency is equal to the natural frequency of spiral waves, a global periodically forced spiral exhibits a drift along a straight line. However, investigation on spiral drift driven by local low-amplitude pacing is still open.

Based on the advantage of local and low-amplitude pacing as well as developing a new method of drift, this paper investigates the spiral motion induced by low amplitude pacing which is localized around the spiral tip. The frequency of local pacing plays a fundamental role in modulating trajectory of the spiral tip. This paper is organized as follows:

1) Introduction (Section 1);
2) Model Presentation (Section 2);
3) Study of spiral motion induced by different frequencies (first part of Section 3). A bifurcations diagram displaying four types of periodic and quasi-periodic spiral patterns is presented. The second part of Section 3 investigates resonant drift when the frequency of pacing is equal to that of the spiral. In the last part of Section 3, a theoretical analysis based on weak deformation approximation is put forward, which confirms the results of numerical simulations;
4) Conclusions and necessary discussions (Section 4).

2. Model

The simulation is based on a two-species modified FitzHugh-Nagumo model (Bär model) of an excitable medium [31]:

$$\frac{\partial u}{\partial t} = f(u,\upsilon) + \Delta u + \sum_{i,j} \gamma_{i,j}\cos(\omega_f t + \phi), \qquad (1)$$

$$\frac{\partial \upsilon}{\partial t} = g(u,\upsilon), \qquad (2)$$

the local reaction kinetics – i.e., the dynamics in the absence of spatial derivatives- is described by:

$$f(u,\upsilon) = -\frac{1}{\varepsilon}u(u-1)\left(u - \frac{\upsilon + b}{a}\right), \qquad (3)$$

$$g(u,\upsilon) = \begin{cases} 0, & 0 \le u < 1/3 \\ -1 - 6.75u(u-1)^2 - \upsilon, & 1/3 \le u \le 1 \\ 1, & u > 1 \end{cases}. \qquad (4)$$

Where u is the activator and υ the inhibitor which represents the variable of a slow recovery process. ε is the ratio of their temporal scales (ε is fixed to 0.02 in the simulation). The dimensionless parameters a and b denote the activator kinetics with b determining the excitation threshold. The spatiotemporal dynamics is investigated by fixing a=0.84 and b=0.07 [31], which make the medium excitable for small positive b and $a < 1 + b$. The last additional term in equation (1) denotes the local pacing, where γ is forcing amplitude and ω_f frequency. The simulation is performed on a square grid with $\Delta x = \Delta y = 0.175$ and with $\Delta t = 0.001$. The pacing is localized in a domain with a radius of R_0=10×Δx around the spiral tip. Accordingly, the summation is computed over a small circular region restricted by $R \le R_0$. Here R is the radius of the disk $R = \sqrt{(x_i - x_0)^2 + (y_i - y_0)^2}$ with (x_0, y_0) the coordinate of the spiral tip and i, j the integer numbers which correspond to the discretized x and y variables as $x_i = (i-1)\Delta x, y_j = (j-1)\Delta y$, respectively. The Euler Scheme is employed on a system with a size of 35×35 with no-flux boundary conditions with the purpose of integrating the equation (1) numerically,

3. Results and discussion

With the fixed parameters, suitable initial conditions lead to readily rotating spiral waves which have been illustrated in Fig. 1(a). In Fig. 1(b), the power spectrum of the intensity time series is obtained from the FFT method. The peak indicates the natural frequency $\omega_0 = 2.24$.

The frequency of the local forcing is critical in modulating the motion of the spiral waves. In Fig. 2, we show the bifurcation diagram which depends on the radius ratio as order parameters and the frequency as control parameters at a fixed weak amplitude $\gamma = 0.05$. When the pacing frequency ω_f, compared to the natural frequency of the spiral, is very small ($\omega_f/\omega_0 < 0.5$), the spiral keeps on rotating around a circle (say, see the orbit at ω_f/ω_0=0.45). Simulation shows that the spiral undergoes a Hopf bifurcation when the ratio ω_f/ω_0 is increased above about 0.5. Simple spirals become unstable and the system undergoes a transition to inward petal meandering spirals (see the path of spiral tip at ω_f/ω_0=0.95 in Fig. 2) which is quasiperiodic. A second cycle with radius r_2 is introduced in this transition. We assume negative values of r_2/r_1 to express hypocycloidlike orbits with inward petals, while we assume plus values to express epicycloidlike orbits with outward petals. The radius expansion of the second circle (r_2) will proceed at an increasing value of ω_f/ω_0 until the spiral drifts along a straight line at ω_f/ω_0=1.0.

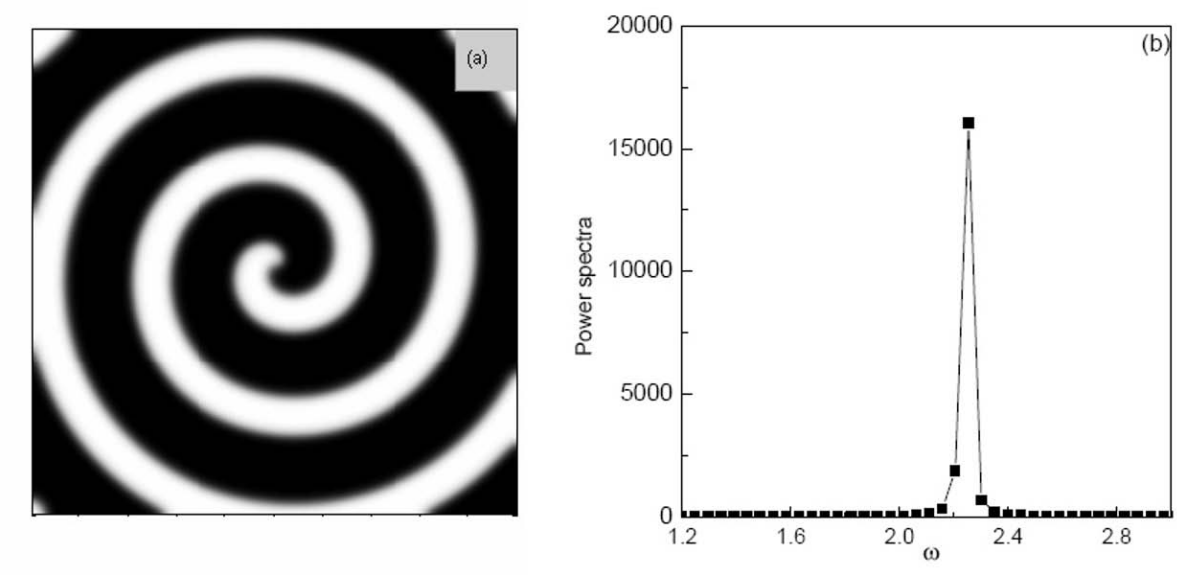

Figure 1. Spiral wave without perturbation. The power spectra of one site (180,180) of system without control shows natural frequency $\omega_0 = 2.24$. parameters are: ε=0.02, a=0.84, b=0.07 [31].

The simulation data shows a dependence:

$$r_2/r_1 = -0.13 + \frac{0.04}{(\omega_f/\omega_0 - 1.01)^2}. \quad (5)$$

It is evident the secondary radius r_2 diverges, yielding a traveling spiral as a critical control parameter value $\omega_f/\omega_0 \approx 1.0$ is approached. Then the relation (5) can be simplified to a scaling relation of $r_2/r_1 \propto (\omega_f/\omega_0 - 1)^{-2}$.

As the ratio ω_f/ω_0 is increased across a critical value of about 1.0, the system shows a transition from traveling spirals to outward petal meandering spirals. In this regime, we find the value r_2/r_1 as a function of ω_f/ω_0 and one which exhibits a similar dependence:

$$y = 0.63 + \frac{0.03}{(x - 0.99)^2}. \quad (6)$$

Thus, the scaling relation $r_2/r_1 \propto (\omega_f/\omega_0 - 1)^{-2}$ with respect to the case ω_f/ω_0 <1.0 is confirmed in the regime ω_f/ω_0 >1.0. When the value is over 1.07, the Hopf bifurcation is eliminated, and the spiral restabilizes.

Now, we focus on the control of resonant drift when the frequency of the local pacing is equal to that of the spiral. The manipulation of the direction and speed of the drift is our main point. In Fig. 3, we present the corresponding trajectories of the spiral tip with different phase shifts at the resonant frequency of $\omega_f = \omega_0$. We first investigated the drift behavior of an counterclockwise rotating spiral wave (see Fig. 3(a), $\sigma = +1$, $\sigma = \pm 1$ represent the chirality of the spiral, σ=+1 for the counterclockwise rotating spiral, while σ=-1 is for the clockwise rotating spiral). Evidently, the direction of the drift can be efficient, guided by the phase shift change of the local pacing. Based on the potential practical application, the optimal selection of the phase shift will be beneficial to force a spiral to drift out of the tissue surface along the shortest path in the least amout of time. Another distinct character is that the drift direction of the spiral waves will change clockwise when we increase the phase shift ϕ of the periodic local pacing. The plotted drift angles θ in Fig. 4(a) show a linear increase with ϕ.

The chirality of the spiral is an important characteristic regarding the investigation of drift dynamics [29]. A change in the chirality of a spiral affects its drift behavior. For example, in the presence of a dc electric field, the component of the drift perpendicular to the electric field changes its sign as the chirality of the spiral wave is changed [28]. Then, we changed the chirality of the spiral from σ=+1 to σ=-1 by reversing the rotating spiral direction. Compared with Fig. 3(a) (σ=+1), trajectories in Fig. 3(b) show similar phenomena while the drift direction changes counterclockwise. Accordingly, one can see that the corresponding values of drift angles θ in Fig. 4(a) decrease linearly as ϕ is increased.

Maintaining the same amplitude of the local pacing, we find the distances of drift in the same period of time (In Fig.

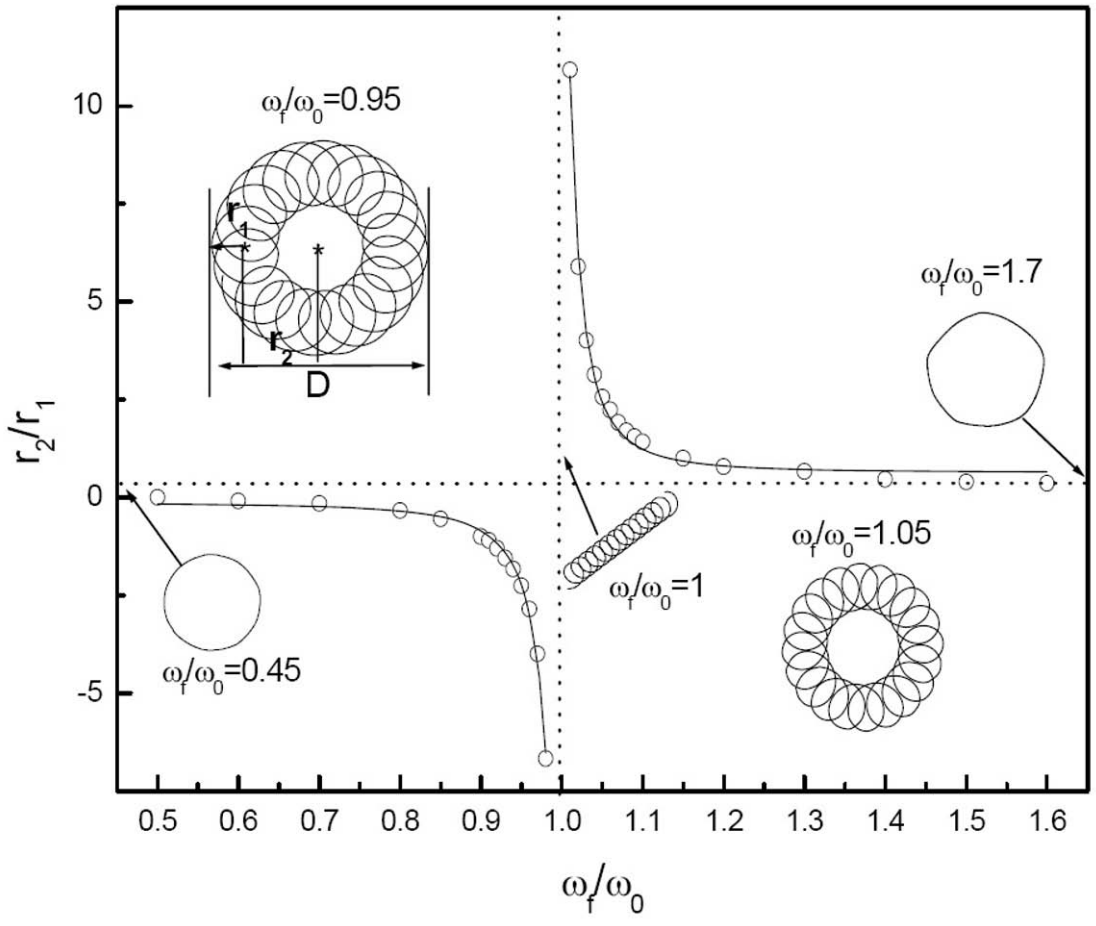

Figure 2. Bifurcations diagram illustrates the transition of trajectories of spiral tip. Ratio r_1/r_2 is controlled by parameter ω_f/ω_0, where r_1 is the average radius of a petal and $r_2 = D/2 - r_1$ (with $D$the outer diameter of the orbit), ω_f the local frequency and $\omega_0 = 2.24$ the natural frequency of spiral respectively. The amplitude of local pacing: γ=0.05. Corresponding orbit is shown: $0 \leq \omega_f/\omega_0 < 0.5$, a circular orbit; $0.5 \leq \omega_f/\omega_0 < 1$, hypocycloidlike orbits with outward petals; $\omega_f/\omega_0 = 1$, a traveling tip; $1.0 \leq \omega_f/\omega_0 \leq 1.7$, epicycloidlike orbits with inward petals; $1.7 < \omega_f/\omega_0$, a circular orbit. The solid curve is drawn by fitting the simulation data (open circles).

3, trajectories are plotted after t=150) almost identical. Compared to Fig. 3(a) and (b), it seems that changing the chirality does not affect the drift velocity. In Fig. 4(b), the plotted drift speed shows an approximate constant value when the phase shift is varied with the settled amplitude both in σ=+1 and σ=-1.

A theoretical analysis will help to attain insight into the underlying mechanism of the resonant drift behavior. Now, with the weak deformation approximation method [32] we will obtain an approximate formulation for the drifting velocity.

We assume that u and υ have a double power series expansion in x and y within at least a small disc around the tip. In polar coordinates, and with rigid rotation at angular velocity ω_0 around the tip [26, 32, 33]:

$$\begin{aligned} u &= u_0 + u_1 r\cos(-\sigma\vartheta + \omega_0 t - \alpha) + o(r^2), \\ \upsilon &= \upsilon_0 + \upsilon_1 r\cos(-\sigma\vartheta + \omega_0 t - \beta) + o(r^2), \end{aligned} \tag{7}$$

Where $u_1 > 0$ and $\upsilon_1 > 0$ are constants; α, β are the two phase shifts. At the origin (the center of the tip's core, which we take as the origin of polar coordinates), $u = u_0$ and $\upsilon = \upsilon_0$; ω_0 is the rotating frequency; $x - x_0(t) = r\cos\vartheta$, $y - y_0(t) = r\sin\vartheta$, where $(x_0(t),y_0(t))$ is the location of the possibly moving tip.

Considering the influence of two arbitrary external fields

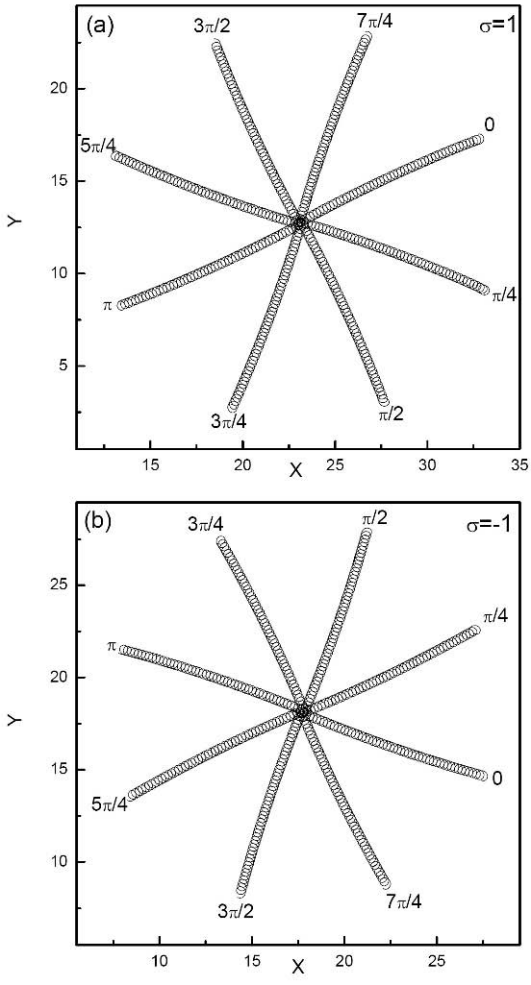

Figure 3. Dependence of the drift by local pacing with amplitude $y = 0.05$on the phase shift at resonant frequency $\omega_f = \omega_0$. (a) tip path of counterclockwise rotating spiral; (b) tip path of clockwise rotating spiral.

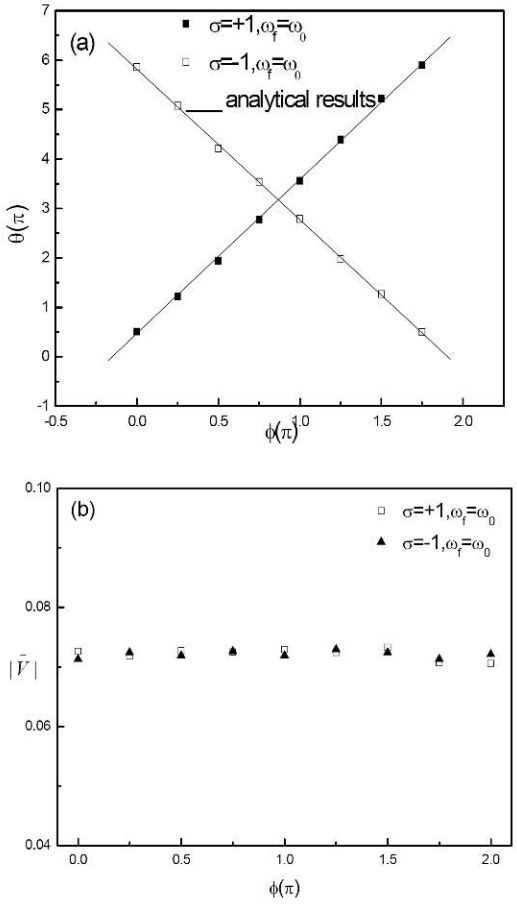

Figure 4. The quantities $|\bar{V}|$ and θ plotted from drift trajectories vs ϕ for the resonant drift of spiral induced by the local pacing at $\omega_f = \omega_0$. The drift angles θ are defined in the following way: choosing the angle between the trajectory at ϕ=0 and the positive x axis as an initial drift angle; when the trajectories rotate clockwise (counterclockwise) as ϕ is increased, we get the angle at different ϕ with respect to trajectory at ϕ=0. Then, adding (subtracting) the angles on the basic initial drift angle.

$\Omega_1(x, y, t)$ and $\Omega_2(x, y, t)$ on the system, we get:

$$\frac{\partial u}{\partial t} = f(u, \upsilon) + \Delta u + \Omega_1, \quad \frac{\partial \upsilon}{\partial t} = g(u, \upsilon) + \Omega_2. \tag{8}$$

Then, we can rewrite the perturbed Eq. (8) in the moving frame of Vunder the assumption that Ω_1 and Ω_2 induce a drift of the spiral wave tip with velocity $V = [V_1(t), V_2(t)]$,

$$\begin{aligned} \frac{\partial u}{\partial t} &= f(u, \upsilon) + \nabla^{2'} u + V \cdot \nabla' u + \Omega_1, \\ \frac{\partial \upsilon}{\partial t} &= g(u, \upsilon) + \Omega_2. \end{aligned} \tag{9}$$

Since Ω_1 and Ω_2 are small and located in a small region around the spiral tip, the deformation of the spiral around the tip is weak. Dense and rigidly rotating spiral waves show numerical results which are reasonable concerning the approximation of the resonant drift induced by external fields [32]. All the values of u, υ, and their derivatives at the tip in the moving frame are kept unchanged compared to those values of the unperturbated spiral (7) at the tip. Based on this approximation, the drift velocity of the spiral tip can be derived (for details see Ref. 32) as:

$$\begin{aligned} V_x(t) &= [(-\Omega_1 \cdot \upsilon_y + \Omega_2 \cdot u_y)/(u_x \upsilon_y - u_y \upsilon_x)]_{tip}, \\ V_y(t) &= [(\Omega_1 \cdot \upsilon_x - \Omega_2 \cdot u_x)/(u_x \upsilon_y - u_y \upsilon_x)]_{tip}, \end{aligned} \tag{10}$$

where$u_x = u_1 \cos(\omega_0 t - \alpha)$, $u_y = \sigma \cdot u_1 \sin(\omega_0 t - \alpha)$, $\upsilon_x = \upsilon_1 \cos(\omega_0 t - \beta)$, $\upsilon_y = \sigma \cdot \upsilon_1 \sin(\omega_0 t - \beta)$, $(u_x \upsilon_y - u_y \upsilon_x) =$

$-\sigma \cdot u_1 v_1 \sin(\beta - \alpha)$. Comparing Eq. (1) with Eq. (8), one can see that $\Omega_1 = \sum_{i,j} \gamma_{i,j} \cos(\omega_f t + \phi)$ and $\Omega_2 = 0$; we get an approximate formula for the drift velocity induced by pacing:

$$V_x(t) = C \cos(\omega_f t + \phi) \sin(\omega_0 t - \beta)$$

$$= \frac{C}{2}[\sin((\omega_f + \omega_0)t + \phi - \beta) - \sin(\omega_f - \omega_0)t + \phi + \beta)],$$

$$V_y(t) = -\sigma \cdot C \cos(\omega_f t + \phi) \cos(\omega_0 t - \beta)$$

$$= -\sigma \cdot \frac{C}{2}[\cos((\omega_f + \omega_0)t + \phi - \beta) + \cos((\omega_f + \omega_0)t + \phi - \beta)]. \quad (11)$$

Where $C = \dfrac{\gamma}{u_1 \sin(\beta - \alpha)}$. Eq. (11) indicates that the spiral waves will get a net drift velocity when the forcing frequency is equal to the natural frequency of the spiral wave, namely $\omega_f = \omega_0$. In this case, Eq. (11) can be simplified as:

$$V_x(t) = \frac{C}{2}[\sin(2\omega_0 t + \phi - \beta) - \sin(\phi + \beta)],$$

$$V_y(t) = -\sigma \frac{C}{2}[\cos(2\omega_0 t + \phi - \beta) + \cos(\phi + \beta)]. \quad (12)$$

Thus, the resonant drift observed in the simulation is confirmed by the theoretical analysis.

The components in Eq. (12) including time are averaged. Then, the path of the tip shows a straight line with net velocity. Consequently, we get a simple expression of the drift speed:

$$\bar{V}_x(t) = -\frac{C}{2} \sin(\phi + \beta),$$

$$\bar{V}_y(t) = -\sigma \frac{C}{2} \cos(\phi + \beta). \quad (13)$$

Thus, the constant drift velocity amplitude $|\bar{V}|$ and the drift angle θ are obtained:

$$|\bar{V}| = \sqrt{\bar{V}_x^2 + \bar{V}_y^2} = \frac{|C|}{2} = \frac{\gamma}{2u_1 \sin(\beta - \alpha)}, \quad (14)$$

$$\tan\theta = \frac{\bar{V}_y}{\bar{V}_x} = \sigma \tan\left(\phi + \beta + \frac{\pi}{2}\right). \quad (15)$$

From Eq. (14), one can see that the drift velocity is directly proportional to the amplitude γ of the periodic pacing. However, it is independent with the phase shift and chirality, consistent with results in Fig. 3 and Fig. 4(b). From Eq. (15), we get the drift angle $\theta = \sigma(\phi + \beta + \frac{\pi}{2}) + k\pi$ which is determined by the phase shift and the chirality of the spiral. Thus, we can conclude that for σ=+1, the drift direction of the spiral waves will change clockwise when the phase ϕ is increased; for σ=-1, the drift direction will change counterclockwise. It is evident that these results are confirmed by the numerical simulations in Fig. 4(a).

4. Conclusion

In conclusion, this paper has investigated the motion of spiral waves controlled by local and low-amplitude pacing. With different frequencies of local pacing imposed on a small domain around a spiral tip, four types of spiral waves motion are observed: rigid rotating, inter meandering, drift spiral, and outer meandering. A scaling relationship of $r_2/r_1 \propto (\omega_f/\omega_0 - 1)^{-2}$ is obtained near the resonant regime. This study looks at the resonant drift when the pacing frequency is equal to that of the spiral. It is shown that the drift velocity and direction can be efficiently controlled by changing the amplitude and phase shift of the local pacing respectively. Theoretical analytical results based on weak deformation approximation are in good agreement with the simulation results. We hope our result will contribute to improving the control scheme with minimizing the damage of tissues. Nevertheless, some problems of crucial importance for the applications to cardiac tissue remain unsolved: the Bär model is a simple monodomain model which is employed in the study of wave propagation in an excitable medium. It ignores the flow of current in the extracellular fluid outside cardiac cells. Real hearts have a nonuniform complex geometry. So, one question is whether the method that has been shown in the simple Bär model could keep its effectiveness in realistic bidomain cardiac models.

Acknowledgements

We wish to thank Prof. Hong Zhang for meaningful discussions. This work was supported by the National Natural Science Foundation of China (Nos. 10747120) and Natural Science Foundation of Zhejiang Province (Nos. Y607525).

References

[1] J. Davidenko, A. Pertsov, R. Salomonsz, W. Baxter, J. Jalife, Nature 355, 349 (1991)
[2] L. Glass, Phys. Today 49, 40 (1996)
[3] A.T. Winfree (Eds.), Focus Issue: Fibrillation in normal ventricular myocardium, Chaos 8 (1998)
[4] B. Benjamin, E. Steinberg, L. Glass, A. Shrier, G. Bub, Phil. Trans. R. Soc. A, 1299, 364 (2006)
[5] M.C. Cross, P.C. Hohenberg, Rev. Mod. Phys. 65, 851 (1993)
[6] B.B. Plapp, D.A. Egolf, E. Bodenschatz, Phys. Rev. Lett. 81, 5334 (1998)

[7] R. Kapral, K. Showalter, Chemical Waves and Patterns (Kluwer, Dordrecht, 1995)
[8] V.K. Vanag, I.R. Epstein, Science 294, 835 (2001)
[9] Q. Ouyang, J.M. Flesselles, Nature 379, 143 (1996)
[10] O. Steinbock, V. Zykov, S.C. Müller, Nature 366, 322 (1993)
[11] S. Alonso, F. Saqués, A. S. Mikhailov, Science 299, 1722 (2003)
[12] D. Barkley, Phys. Rev. Lett. 72, 164 (1994)
[13] R.A. Gray, A.M. Pertsov, J. Jalife, Nature 392, 75 (1998)
[14] J.M. Davidenko, A. M. Pertsov, R. Salomonsz, W. Baxter, J. Jalife, Nature 355, 349 (1992)
[15] I. Aranson, H. Levine, L. Tsimring, Phys. Rev. Lett. 72, 2561 (1994)
[16] N.J. Wu, H. Zhang, H.P. Ying, Z.J. Cao, G. Hu, Phys. Rev. E 73, R060901 (2006)
[17] L. W. Piller, Electronic Instrumentation Theory of Cardiac Technology (Staples Press, London, 1970)
[18] L. Tung, Proc. IEEE 84, 366 (1996)
[19] V.N. Biktashev, A.V. Holden, J. Theor. Biol. 169, 101 (1994)
[20] A.V. Panfilov, S.C. Müller, V.S. Zykov, J.P. Keener, Phys. Rev. E 61, 4644 (2000)
[21] M. Vinson, S. Mironov, S. Mulvey, A. Pertsov, Nature 386, 477 (1997)
[22] H. Zhang, Z.J. Cao, N.J. Wu, H.P. Ying, G. Hu, Phys. Rev. Lett. 94, 188301 (2005)
[23] Z.J. Cao, P.F. Li, H. Zhang, F. G Xie, G. Hu, Chaos 17, 0151071 (2007)
[24] V.I. Krinsky, K.I. Agladze, Physica D 8, 50 (1983)
[25] O. Steinbock, V. Zykov, S.C. Müller, Nature 366, 322 (1993)
[26] H. Zhang, N.J. Wu, H.P. Ying, G. Hu, B. Hu, J. Chem. Phys. 121, 7276 (2004)
[27] M. Markus, Zs. Magy-Ungvaray, B. Hess, Science 257, 225 (1992)
[28] O. Steinbock, J. Schütze, S.C. Müller, Phys. Rev. Lett. 68, 248 (1992)
[29] A.P. Munuzuri, M. G. Gesteira, V.P. Munuzuri, V.I. Krinsky, V. P. Villar, Phys. Rev. E 50, 4258 (1994)
[30] K.I. Agladze, V.A. Davydov, A.S. Mikhailov, JETP Lett. 45, 767 (1987)
[31] M. Bär, M. Eiswirth, Phys. Rev. E 48, R1635 (1993)
[32] H. Zhang, B. Hu, G. Hu, J.H. Xiao, J. Chem. Phys. 119, 4468 (2003)
[33] M. Wellner, A.M. Pertsov, J. Jalife, Phys. Rev. E 59, 5192 (1999)